P5R.8

RETRIEVAL OF VERTICAL RAIN RATE PROFILE BY DUAL-FREQUENCY RADAR DATA

Koyuru Iwanami *[1], Yohei Chono [2], Toshio Harimaya [2], Jacques Testud [3],
Masayuki Maki [1], Ryohei Misumi [1], Sang-Goon Park [1]
1: National Research Institute for Earth Science and Disaster Prevention (NIED), Tsukuba, Japan
2: Hokkaido University, Sapporo, Japan
3: NOVIMET, Vélizy, France

1. INTRODUCTION

Based on the success of the TRMM mission, GPM (Global Precipitation Measurement) mission was proposed. A dual-frequency precipitation radar (DPR) on the core satellite of GPM is expected to play a significant role in the mission (Iguchi, 2003).

Testud (2004) described that there were two approaches, that is, "differential" (Iguchi and Meneghini 1995) and "integral" (Meneghini and Nakamura 1990) techniques in dual-frequency algorithm for the retrieval of rain rate profile.

In this study, retrieval algorithm of vertical rain rate profile by dual-frequency radar was proposed in line with integral approach and applied to the NIED ground-based radar data.

2. ALGORITHM

The developed retrieval algorithm of vertical rain rate profile by dual-frequency radar uses a mutual constraint that expresses the consistency of the along path attenuations over a common segment sampled at the two frequencies and the assumption that N_0^* is constant along the profile (Testud, 2004).

2.1 *Relationships between DSD Moments*

The inverse model consists of three relationships between two of reflectivity factor Z in mm^6m^{-3}, specific attenuation A in $dBkm^{-1}$ and rain rate R in mmh^{-1} normalized by the normalized intercept parameter N_0^* of DSD (drop size distribution) of rain in the proposed algorithm. N_0^* is defined as

$$N_0^* = \frac{4^4}{\pi\rho_w}\frac{\mathrm{LWC}}{D_m^4}, \quad (1)$$

where LWC is the liquid water content, ρ_w is the density of liquid water and D_m is the mean volume diameter (ratio of the fourth to the third moment of the DSD). N_0^* represents the intercept parameter N_0 of the exponential distribution with the same LWC and D_m, whatever the shape of the DSD (Testud et al. 2001). It was shown in Testud et al. (2000) that quasi-universal relationships were established between any couple of integral parameters of the DSD after the normalization by N_0^* and the relationships might be satisfactorily approximated by power laws. The following representations were used as the inverse model for the retrieval:

$$A = aN_0^{*(1-b)}Z^b, \quad (2)$$

$$R = cN_0^{*(1-d)}Z^d, \quad (3)$$

$$R = eN_0^{*(1-f)}A^f, \quad (4)$$

where a, b, c, d, e and f are the coefficients dependent on the temperature. These coefficients at X-, Ka- and W-band were derived from Z and A calculated by the T-Matrix method (Mishchenko et al. 2000, 2002) and R using DSD data. DSD data were measured by ORS (Optical Raindrop Spectrometer) and the RD-69 disdrometers at several sites in Japan from 1996 to 2003. The calculation was done on the conditions of 15 °C temperature, axis ratio by Andsager et al. (1999), terminal velocity approximated by Atlas and Ulbrich (1977) of raindrop.

The coefficients in the relationships (2) to (4) were derived by the least square fitting from scatter plots such as Fig. 1. It was found that uncertainty of the relationships could be decreased by the normalization comparing top with bottom panels in Fig. 1. Hereafter the combination of X- and Ka-band radar data will be considered because the effect of moment of DSD strongly appeared at W-band. The differences of the coefficients with DSD observation sites were small.

2.2 *Retrieval Algorithm*

The apparent (attenuated) radar reflectivity Z_a can be represented by the equivalent radar reflectivity Z_e and specific attenuation A as

$$Z_a(r) = Z_e(r)\exp\left[-0.46\int_0^r A(u)du\right], \quad (5)$$

where r is the range from the radar. Hitschfeld and Bordan (1954) showed the solution of (5) is

$$A(r_i) = \frac{A(r_n)Z_a^b(r_i)}{Z_a^b(r_n) + A(r_n)I(r_i, r_n)}, \quad (6)$$

where

$$I(r_i, r_n) = 0.46b\int_{r_i}^{r_n} Z_a^b(u)du. \quad (7)$$

This means that the specific attenuation profile $A(r_i)$ along segment $[r_0,r_n]$ is the function of the profile $Z_a(r_i)$ and the value of A at the far bound r_n.

Here it was assumed that N_0* was constant along

* *Corresponding author address:* Koyuru Iwanami, National Research Institute for Earth Science and Disaster Prevention (NIED), Tsukuba 305-0006 Japan; e-mail: iwanami@bosai.go.jp

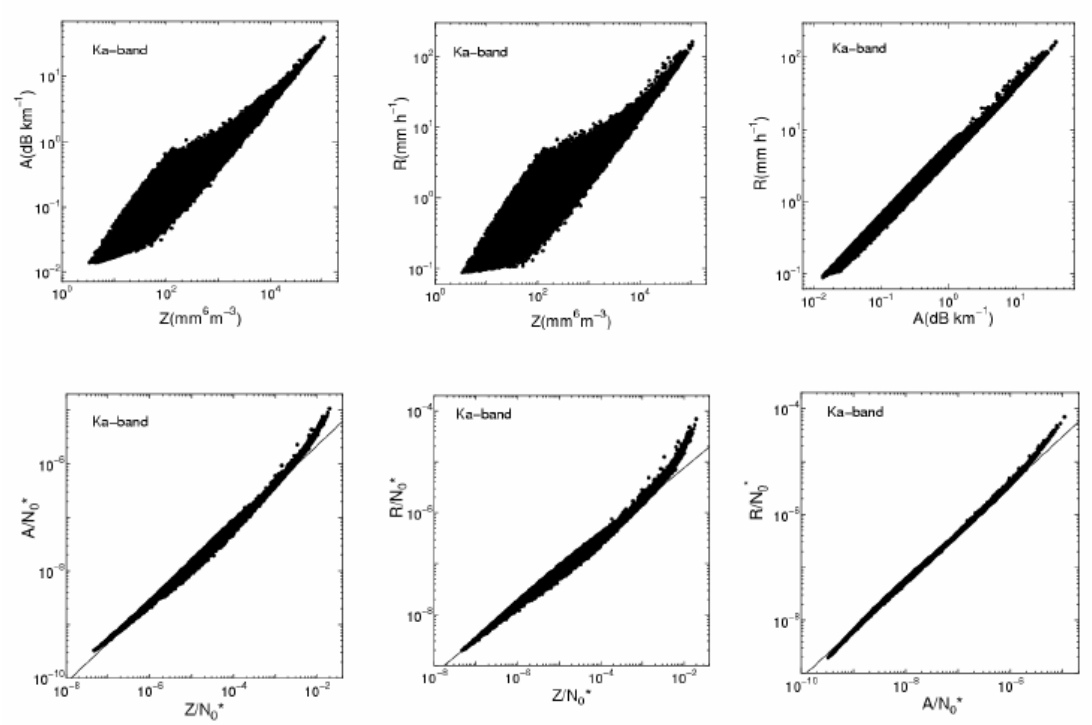

FIG. 1. Scatter plots of relationships between A and Z (left), R and Z (center), and R and A (right) before (top) and after (bottom) the normalization by N_0^* at Ka-band. Each parameter was calculated by T-matrix method using observed DSD data.

the segment $[r_0,r_n]$. Testud et al. (2001) demonstrated that the variability of N_0^* was essential from event to event and this variability was much more moderate within one particular event after separating convective and stratiform rain. Then N_0^* in the segment $[r_0,r_n]$ can be expressed as

$$N_0^* = \left[\frac{1-\exp(-0.46bQ)}{aI(0,r_n)}\right]^{1/(1-b)}, \qquad (8)$$

where

$$Q = \int_0^{r_n} A(u)du. \qquad (9)$$

Our retrieval algorithm by dual-frequency radar utilizes a mutual constraint that expresses the consistency of the along path attenuations over a common segment sampled at the two frequencies (Testud, 2004), which can be expressed as

$$\int_{r_0}^{r_n} A_2(u)du = \int_{r_0}^{r_n} pN_0^{*(1-q)}A_1^q(u)du, \qquad (10)$$

where $[r_0,r_n]$ represent a common interval of data sampled by the two frequencies, and

$$A_2 = pN_0^{*(1-q)}A_1^q \qquad (11)$$

is the power low relationship relating the specific attenuations at two frequencies. Subscript 1 and 2 indicates the lower and higher frequency, respectively. The coefficients p and q were also derived from T-Matrix calculation using DSD data. Figure 2 shows scatter plots of relationship between specific attenuations at the X- and Ka-band before and after the normalization by the N_0*.

The retrieval procedure depicted in Fig. 3 is as

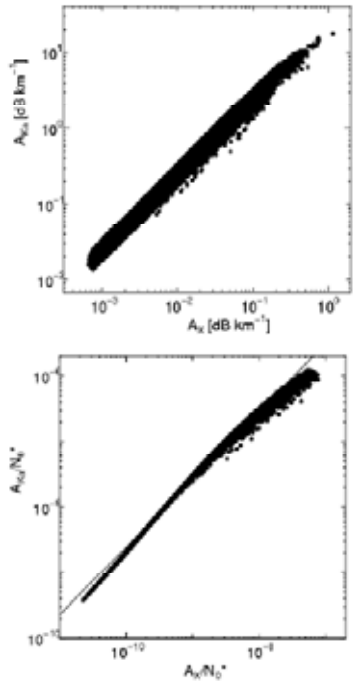

FIG. 2. Scatter plots of relationships between specific attenuations A at Ka- and X-band before (top) and after (bottom) the normalization by N_0^*. Values of A were calculated by T-matrix method using observed DSD data.

follows. Subscript *X* and *Ka* shows X- and Ka-band, respectively.

(i) First specific attenuation $A_X(r_n)$ at the far bound r_n at X-band is assumed and the vertical profile $A_X(r_i)$ is calculated by the observed profile of $Z_{aX}(r_i)$ through (6).

(ii) Q_X is calculated from profile $A_X(r_i)$ then $N_0{}^*{}_X$ is derived from Q_X and $Z_{aX}(r_i)$.

(iii) $A_{Ka}(r_n)$ at the far bound r_n at Ka-band is assumed and the vertical profile $A_{Ka}(r_i)$ is calculated by the observed profile of $Z_{aKa}(r_i)$ in the same way as (i).

(iv) $N_0{}^*{}_{Ka}$ is calculated as in (ii).

(v) $A_{Ka}(r_n)$ which makes $N_0{}^*{}_{Ka}$ equal to $N_0{}^*{}_X$ is derived by comparing them in (ii) and (iv). So far a set of $A_{Ka}(r_n)$ and $N_0{}^*$ for one $A_X(r_n)$ can be determined.

(vi) A set of $A_X(r_i)$ and $A_{Ka}(r_i)$ calculated from $A_X(r_n)$ and $A_{Ka}(r_n)$ with $N_0{}^*$ in (v) is estimated by the mutual constraint of (10) and the best set of $A_X(r_n)$, $A_{Ka}(r_n)$ and $N_0{}^*$ is selected.

(vii) Rain rate profile $R(r_i)$ is calculated from the $A(r_n)$ and $N_0{}^*$ by (4). Two profiles of $R_X(r_i)$ and $R_{Ka}(r_i)$ can be available from the $A_X(r_i)$ and $A_{Ka}(r_i)$, respectively.

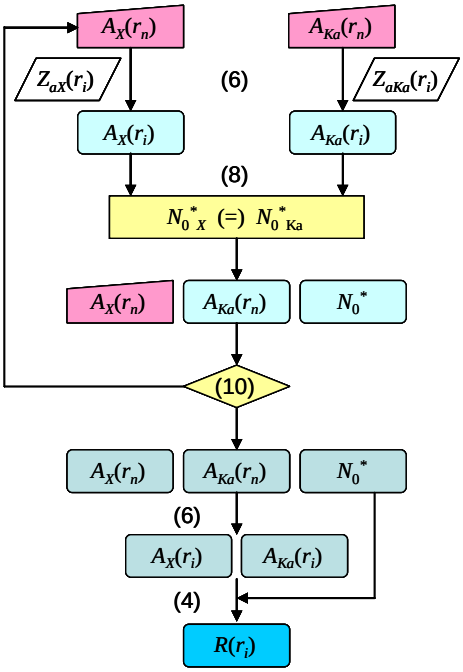

FIG. 3. Schematic chart of the proposed algorithm. Numbers in parentheses indicate equations in text.

3. RESULTS

3.1 *Model Calculations*

In order to verify the developed rain rate retrieval algorithm by dual-frequency radar data, it was tested by the model calculations before its application to observed radar data. The test profiles of apparent reflectivity factor, $Z_a(r_i)$ at X- and Ka-band were made by calculated reflectivity factor $Z_e(r_i)$ and specific attenuation $A(r_i)$ from assumed profiles of rain rate $R_O(r_i)$ and $N_0{}^*$. Then rain rate profiles were retrieved from the test data of apparent reflectivity factor profiles. The value of rain rate on the ground surface $R_O(0)$ and $N_0{}^*$ was set to 7.006 mmh^{-1} and 2.045×10^7 m^{-4}, respectively. Three profiles of $R_O(r_i)$ which was constant, increasing and decreasing with height were assumed.

Figure 4 indicates the retrieval results for three types of rain rate profiles. Left panels show the $Z_a(r_i)$ at X- and Ka-band, and right panels show model $R_O(r_i)$, retrieved $R_X(r_i)$ and $R_{Ka}(r_i)$ together with $R_{MP}(r_i)$ calculated by *Z-R* relationship ($Z=200R^{1.6}$) using $Z_{aX}(r_i)$.

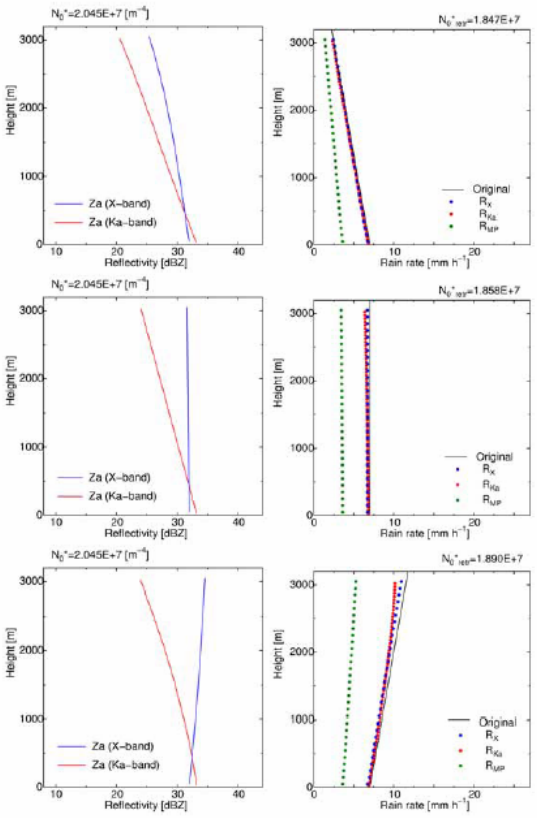

FIG. 4. Left panels show the profile of apparent reflectivity factor $Z_a(r_i)$ at X- (blue) and Ka-band (red) calculated from model profile of rain rate $R_O(r_i)$ (black line) in the right panels and $N_0{}^*$. Right panels indicates retrieval results of rain rate profiles of $R_X(r_i)$ (blue dots) and $R_{Ka}(r_i)$ (red dots), together with $R_{MP}(r_i)$ estimated by *Z-R* relationship (green dots) for three model profiles of $R_O(r_i)$.

Although the retrieved rain rate profiles had tendency to slightly underestimate, they could estimate model profiles accurately and were much

better than by *Z-R* relationship. The maximum retrieved errors at the highest level (3000 m) were 5 and 11 % for R_X and R_{Ka} for the model profile increasing with height. For the model profiles constant and increasing with height, R_{Ka} could retrieve more accurately than R_X in the lower altitude (that is, near the radar) but vice versa in the higher altitude.

It was possible to replace (i) and (ii) with (iii) and (iv) in the order of retrieval procedure described in the previous section, but the retrieval errors became larger.

The accurate data near the ground surface could not obtained by ground-based radars because of the hardware limitation and ground clutter. In the case without data near the ground surface, it was also possible to retrieve rain rate profile with small error by assuming constant rain rate of measured value on the ground in the range of no data.

3.2 *Application to Observed Data*

The proposed algorithm was applied to the observed data. A field experiment named Vertically Pointing Measurements, Tsukuba, 2001 (VPM_TKB01) was carried out by using the ground-based triple-band multiparameter radar system (Iwanami et al. 2001) at the NIED (36.12N, 140.09E) in Tsukuba, Japan during June 12 to July 8, 2001. Three radars MP-X and MP-Ka/W continuously measured vertical profiles by PPI scans of 90 degree elevation. The range resolution was 100 m for MP-X and 50 m for MP-Ka/W radars and the number of pulse integration was 256. The retrieval algorithm was applied to one minute average radar data after Ka-band data were set to 100 m resolution data. Rain rate data by disdrometer RD-69 on the ground were also used for the retrieval.

Figure 5 shows time height cross sections of the observed Z_{aX} (top), Z_{aKa} (middle), and retrieved rain rate (bottom) from 11:43 to 11:51 JST on June 21, 2001. It was found that reasonable rain rate profiles were derived but for 11:43.

4. DISCUSSIONS

It was assumed that N_0* is constant along the segment $[r_0,r_n]$ in this algorithm. Sensitivity tests for N_0^* variations by 10, 50 % and one order with height were made. Calculations were made for the same three rain rate profiles as in Fig. 4, and $Z_a(r_i)$ were made for two cases that N_0^* in the height range upper than 1500 m ($N_{0\,H}^*$) was larger and smaller than that below 1500 m ($N_{0\,L}^*$). Results for the constant rain rate profile in case of $N_{0\,H}^* > N_{0\,L}^*$ and $N_{0\,H}^* < N_{0\,L}^*$ were shown in Fig. 6 and 7, respectively.

In case of $N_{0\,H}^* > N_{0\,L}^*$, retrieved rain rate profiles underestimated (Fig. 6), on the other hand overestimated in upper level and underestimated in lower level in case of $N_{0\,H}^* < N_{0\,L}^*$ (Fig. 7). The errors of retrieved rain rate in the higher levels were less than about 10, 15, and 50 % for N_0^* variations by 10, 50 % and one order, respectively. The effect of the

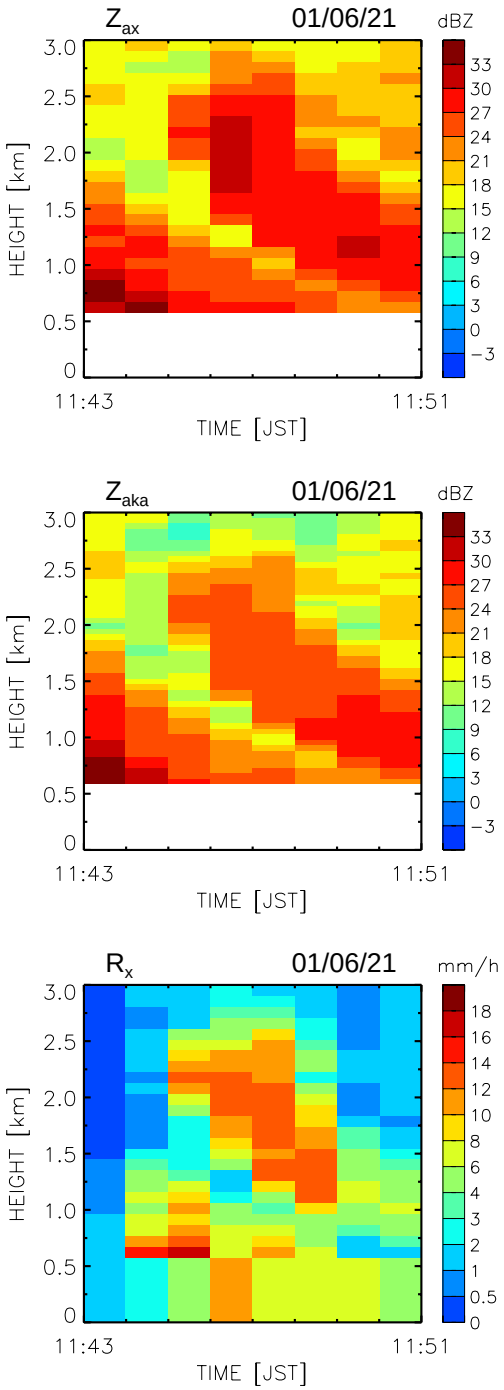

FIG. 5. Time height cross sections of the observed Z_{aX} (top), Z_{aKa} (middle), and retrieved rain rate (bottom) from 11:43 to 11:51 JST on June 21, 2001.

N_0^* variations on the retrieval results were not large. Retrieval errors in case of $N_{0\,H}^* > N_{0\,L}^*$ were larger than $N_{0\,H}^* < N_{0\,L}^*$ by about 5 %. It was also found that the retrieval error could be suppressed by the application of the retrieval for each segment, if the height of N_0^*

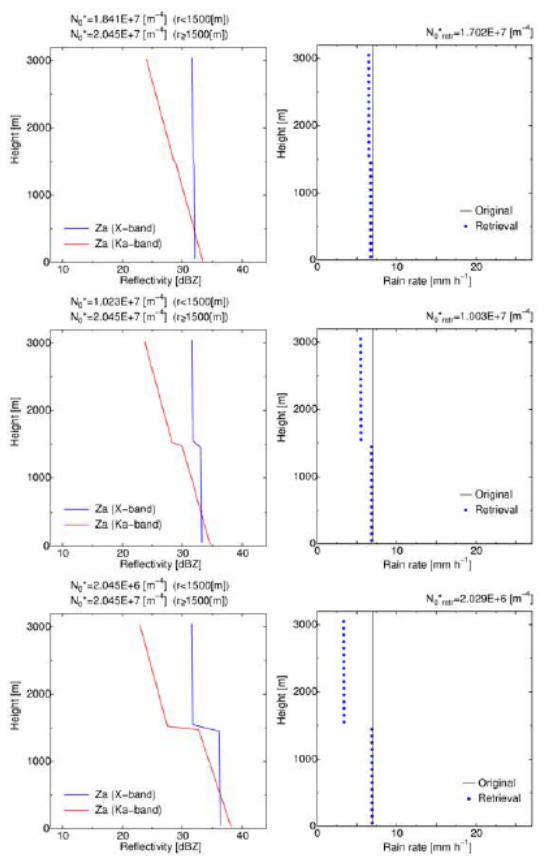

FIG. 6. Same as Fig. 4 but for only the constant rain rate profile with height in case of $N_{0\,H}^{*} > N_{0\,L}^{*}$. Only the model (black line) and retrieved $R_X(r_i)$ (blue dots) rain rate profiles are shown in the right panels.

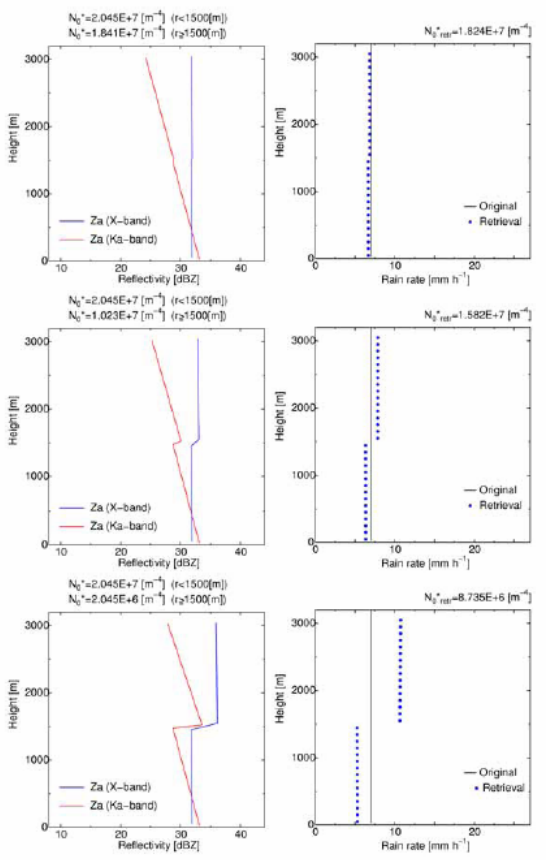

FIG. 7. Same as Fig. 6 but for in case of $N_{0\,H}^{*} < N_{0\,L}^{*}$.

change was known (figures not shown). This suggests that the segmentation of the ray like the ZPHI algorithm (Testud et al. 2000) may improve the proposed retrieval algorithm.

5. SUMMARY

Retrieval algorithm of vertical rain rate profile by dual-frequency radar was developed and applied to the NIED ground-based radar data. The algorithm uses a mutual constraint that expresses the consistency of the along path attenuations over a common segment sampled at the two frequencies and the assumption that N_0^* is constant along the profile (Testud, 2004).

Relationships between two of reflectivity factor, specific attenuation and rain rate normalized by the normalized intercept parameter N_0^* (Testud et al. 2001) at X-, Ka- and W-band were obtained by T-Matrix calculations using DSD data measured with disdrometers at several sites in Japan. Uncertainty of the relationships could be decreased by the normalization although the effect of moment of DSD strongly appeared at W-band.

The proposed algorithm was tested by model calculations. The test profiles of apparent reflectivity factor were made by calculated reflectivity factor and specific attenuation from assumed profiles of rain rate and N_0^*. Then rain rate profiles were retrieved from the test data of apparent reflectivity factor profiles. The retrieved errors were less than 5 % and larger at higher altitude because of the accumulated error of attenuation estimation but results were much better than by *Z-R* relationship.

Sensitivity tests for N_0^* variations by 10, 50 % and one order with height were also made and errors of retrieved rain rate were less than about 10, 15, and 50 %, respectively. If the height of N_0^* change was known, the retrieval error could be suppressed. In the case without data near the ground surface, it was possible to retrieve rain rate profile with small error by assuming constant rain rate in the range of no data by measured rain rate on the ground.

The proposed algorithm was applied to the data observed by the NIED X- and Ka-band radars in Tsukuba city, Japan in June 2001 and reasonable rain rate profiles were derived. It is necessary to calibrate radar reflectivity well to retrieve rain rate accurately.

ACKNOWLEDGEMENTS

This work has been partly supported by CREST (Core Research for Evolutional Science and Technology) of JST (Japan Science and Technology Corporation) entitled “GSMaP: Global Satellite Mapping of Precipitation.” The authors thank Dr. Akihiro Hashimoto from AESTO (Advanced Earth Science and Technology Organization), Japan for his providing DSD data measured by the Optical Raindrop Spectrometer and those analysis programs.

REFERENCES

Andsager, K., K. V. Beard, and N. F. Laird, 1999: Laboratory measurements of axis ratios for large raindrops. *J. Atmos. Sci.*, **56**, 2673-2683.

Atlas, D., and C. W. Wlbrich, 1977: Path- and area-integrated rainfall measurement by microwave attenuation in the 1-3 cm band. *J. Appl. Meteor.*, **16**, 1322-1331.

Hitschfeld, W., and J. Bordan, 1954: Errors inherent in radar measurement of rainfall at attenuating wavelengths. *J. Meteor.*, **11**, 58-67.

Iguchi, T., 2003: Spaceborne precipitation radars in TRMM and GPM. *Proc. 31st Conf. Radar Meteor.*, 371-374.

Iguchi, T., and R. Meneghini, 1995: Differential equations for dual-frequency radar returns. *Proc. 27th Conf. Radar Meteor.*, 190-193.

Iwanami, K., R. Misumi, M. Maki, T. Wakayama, K. Hata, and S. Watanabe, 2001: Development of a multiparameter radar system on mobile platform. *Proc. 30th Intern’l Conf. Radar Meteor.,* 104-106.

Meneghini, R., and K. Nakamura, 1990: Range profiling of the rain rate by an airborne weather radar. *Remote Sensing Environ.*, **31**, 193-209.

Mishchenko, M. I., J. W. Hovenier, and L. D. Travis, 2000: *Light Scattering by Nonspherical Particles*. *Academic Press*., 690pp.

Mishchenko, M. I., L. D. Travis, and A. A. Lacis, 2002: *Scattering, Absorption and Emission of Light by Small Particles*. *Cambridge Univ. Press*. 445pp.

Testud, J., 2004: Precipitation measurements from space. *Weather Radar*, *Springer*, 199-234.

Testud, J., E. Le Bouar, E. Obligis, and M. Ali-Mehenni, 2000: The rain profile algorithm applied to polarimetric weather radar. *J. Atmos. Ocean. Tech.*, **17**, 332-356.

Testud, J., S. Oury, R. A. Black, P. Amayenc, and X. Dou, 2001: The concept of ”normalized” distribution to describe raindrop spectra: A tool for cloud physics and cloud remote sensing. *J. Appl. Meteor.*, **40**, 1118-1140.